Attenuating ABHD17 enhances *S*-palmitoylation, membrane localization and signal transduction of NOD2 and Crohn's disease-associated variants.

Charneal L. Dixon[1,2], Noah R. Martin[1], Micah J. Niphakis[3], Benjamin F. Cravatt[4], Gregory D. Fairn[1,2,5,6*]

[1]Department of Pathology, Dalhousie University, Halifax, NS, Canada

[2]Keenan Research Centre for Biomedical Science, St. Michael's Hospital, Unity Health Toronto, Toronto, ON, Canada

[3]Lundbeck La Jolla Research Center, Inc., San Diego, CA, USA

[4]Department of Chemistry, The Scripps Research Institute, La Jolla, CA, USA

[5]Department of Biochemistry and Molecular Biology, Dalhousie University, Halifax, NS, Canada

[6]Lead Contact

*Correspondence: gfairn@dal.ca

SUMMARY

NOD2 is an intracellular innate immune receptor that senses bacterial peptidoglycans. Although soluble in the cytosol, a portion of the protein is associated with the plasma membrane and endosomal compartments for microbial surveillance. Palmitoylation of NOD2 by zDHHC5 promotes its membrane recruitment to drive proinflammatory and antimicrobial responses to pathogenic invasion. A depalmitoylation step by an unknown protein, thioesterase, releases NOD2 from membranes into the cytosol, where the protein can then enter a new cycle of palmitoylation-depalmitoylation. Here, we identify α/β-hydrolase domain-containing protein 17 isoforms (ABHD17A, 17B, 17C) as the thioesterases responsible for depalmitoylation of NOD2. Inhibiting ABHD17 increased the plasmalemmal localization of both wild-type NOD2 and a subset of hypo-palmitoylated Crohn's disease-associated variants, resulting in increased NF-κB activation and production of pro-inflammatory cytokines in epithelial cells. These results suggest that targeted inhibition of ABHD17 may rescue some Crohn's disease-associated NOD2 variants.

Keywords: *S*-palmitoylation, NOD2, ABHD17, Crohn's disease, intestinal epithelial, IL-8

INTRODUCTION

Crohn's disease (CD) is a prominent form of inflammatory bowel disease that can affect any segment of the gastrointestinal tract, extending from the mouth to the anus. However, it most commonly manifests in the lower portion of the small intestine and the upper colon. CD is characterized by a range of symptoms, including weight loss, fatigue, diarrhea, and abdominal pain, which can be debilitating and, in some instances, life-threatening. Present-day treatments, including the use of steroids and tailored dietary approaches, have proven effective in alleviating these symptoms and forestalling disease exacerbations. Despite these advances, CD remains an intricately multifaceted condition influenced by genetic predisposition, environmental factors, dietary habits, and an individual's unique microbiome.

The nucleotide-binding oligomerization domain (NOD)-like receptor 2 (NOD2) gene has been consistently implicated in the pathogenesis of CD since it was first identified in 2001 [1-3]. NOD2 is a member of the evolutionarily conserved family of NOD-like receptors (NLR) that provide intracellular surveillance through detecting cytoplasmic pathogen-associated molecular patterns [4-6]. NOD2 belongs to the NLRC subfamily as it contains two amino terminal caspase activation and recruitment domains (CARD) [7]. NOD2 and the closely related NOD1 are able to bind small peptides originating from bacterial peptidoglycan. Peptidoglycan fragment binding and NOD2 oligomerization result in the engagement of receptor-interacting protein kinase 2 (RIPK2) that in turn leads to a series of ubiquitination and phosphorylation events that trigger the activation of nuclear factor kappa B (NF-κB) and mitogen-activated protein kinases (MAPK)

pathways, that ultimately lead to transcriptional induction of pro-inflammatory cytokines, chemokines and additional inflammatory mediators [8,9].

The complex pathophysiology of CD has led to the emergence of multiple functional roles for NOD2. In the presence of a diverse and healthy microbiome, NOD2 is thought to provide signals that facilitate the expression and secretion of small anti-microbial peptides (AMPs), termed α- and β-defensins by Paneth cells and other epithelial cells of the small and large intestine [10,11]. Thus, loss of NOD2 function and a reduction in the complement of AMPs can lead to changes in the microbiome and dysbiosis. This shift in the bacterial population and activity can result in an increase in bacteria capable of damaging or invading the epithelial lining. In this instance, NOD2 also plays a critical role in combination with ATG16L1, another CD risk factor, in initiating an anti-bacterial autophagic pathway in response to invasion [12-14]. Finally, NOD2 can be exposed to peptidoglycan in resident macrophage and epithelial cells through the uptake of peptidoglycan through the SLC15A family of transporters located in the plasma membrane (PM) and endosomes [15-17]. However, whether loss of this NOD2 function contributes to CD is less clear, but could impact the ability of patients to recover from acute infections, as seen in murine models [18].

In contrast to toll-like receptors that recognize bacterial components at the cell surface or in the lumen of endosomes, NOD2 is an intracellular receptor that associates with the PM or endosomal compartments to detect bacterial peptidoglycan after its transport to the cytoplasm [17]. Whereas several protein interaction partners for NOD2 have been described that could conceivably help target the protein to the PM and endosomes, it was previously demonstrated that *S*-palmitoylation (or *S*-acylation), a

reversible post-translational modification, was required to target NOD2 and NOD1 to membranes [19,20]. It was further revealed that the protein acyltransferase zDHHC5 mediated the attachment of the fatty acyl group to NOD2 (Cys395 and 1033) and NOD1 (Cys558, 567, 952) critical for NODs to respond to peptidoglycan and mount an effective immune response [19]. Additionally, several CD-associated loss-of-function variants of NOD2 displayed reduced levels of *S*-palmitoylated, which we refer to as hypo-palmitoylated. For these hypo-palmitoylated variants, the relative lack of *S*-palmitoylation correlated with decreased signaling in response to peptidoglycan. We speculated that identifying and inhibiting the responsible thioesterase(s) could conceivably increase the *S*-palmitoylation of not only wild-type NOD2 but some hypo-palmitoylated mutants. Indeed, such an intervention could improve the functionality of some of the CD-associated NOD2 mutants.

In this study, we identify the family of α/β-hydrolase domain-containing protein 17 (ABHD17A, 17B, 17C) as the enzymes responsible for the depalmitoylation of NOD2. Furthermore, we find that inhibiting ABHD17 enzymes partly restores the localization, *S*-palmitoylation and ligand-induced signaling of a subset of CD-associated loss-of-function NOD2 variants.

RESULTS

Depalmitoylation of NOD2 is enzymatically mediated

Unlike other types of protein lipidation, the covalent attachment of palmitate and other fatty acids to Cys residues via a thioester bond can be reversible [21]. Dynamic changes in the *S*-palmitoylation status can contribute to protein regulation and function

[22-24]. Indeed, the fraction of NOD1 and NOD2 that are *S*-palmitoylated is increased in response to stimuli [19]. Yet, to date, nothing is known about the reversibility of this modification on NOD2 or the identity of a thioesterase/depalmitoylation enzyme. To determine if colorectal epithelial cells express a thioesterase capable of depalmitoylating NOD2, we first developed a cell model with controllable low-level expression of NOD2. To do this, we used the Sleeping Beauty transposon system to engineer an HCT116 cell line with a doxycycline-inducible GFP-tagged NOD2 (GFP-NOD2) as described in the Methods. Following the generation and selection of the polyclonal cell line, doxycycline-inducible expression of GFP-NOD2 was confirmed by immunoblotting and microscopy (Figure 1*A*, *B*). In these cells, there was a sizeable cytosolic pool of GFP-NOD2, and a smaller fraction associated with the PM, consistent with previous results [19,25,26]. Palmostatin B is a cell-permeable, broad-spectrum inhibitor that targets multiple depalmitoylases including acyl protein thioesterase (APT) 1 and 2 [27,28], palmitoyl-protein thioesterase 1 [28], a/b-hydrolase domain (ABHD) 6 [29], ABHD10 [30] ABHD12 [31], ABHD16A [29,32] and ABHD17(A/B/C) [29]. Thus, we next treated cells expressing GFP-NOD2 with either solvent control (DMSO) or Palmostatin B for 4 h. Following the 4 h incubation with Palmostatin B, confocal microscopy revealed a significant 3.4-fold enrichment of the GFP-NOD2 on the PM (p=0.0097) (Figure 1*C*, *D*). Since it was previously demonstrated that NOD2 mutants incapable of being palmitoylated are completely cytosolic [19,20], we reasoned that the observed plasmalemmal enrichment was due to a more significant fraction of GFP-NOD2 being *S*-palmitoylated. To confirm this experimentally, we used an acyl resin-assisted capture (acyl-RAC) technique (Figure 1*E*) that uses a series of steps, including the blockage of

free-thiols, cleavage of acyl-thioester bonds, and the use of an affinity matrix to bind the newly liberated and previously *S*-palmitoylated Cys residues from cell lysates. Immunoblotting GFP-NOD2 following acyl-RAC demonstrated a 2.5-fold increase (p=0.03) in palmitoylated GFP-NOD2 in cells treated with Palmostatin B compared to control (Figure 1*F*). The presence of a signal with hydroxylamine (NH_2OH) treatment indicates that the attachment of palmitate to the protein is via a thioester bond. These results suggest that *S*-palmitoylation of NOD2 is reversible and that a Palmostatin B-sensitive protein mediates the enzymatic removal of palmitate from NOD2.

Inhibiting ABHD17 enzymes increases NOD2 palmitoylation

Motivated by the impact of Palmostatin B on NOD2 localization and *S*-palmitoylation, we used selective small-molecule inhibitors to target eight known depalmitoylation enzymes with the goal of identifying the relevant NOD2 thioesterases. HCT116 cells stably expressing GFP-NOD2 were treated with DMSO vehicle or inhibitor for a total of 4 h. Treatment with ML348 [33] and ML349 [33], which target APT1 and APT2 respectively, had no discernable effect on the localization of GFP-NOD2 (Figure 2*A*). A similar lack of response was observed with the selective ABHD6 inhibitor, WWL70 [34,35]. Conversely, THL [35,36] and ABD957[37] treated cells have significant enrichment of GFP-NOD2 at the PM, 2.2-fold (p=0.0175) and 4.9-fold (p<0.0001) increase, respectively (Figure 2*B*). For ABD957 treated cells, this corresponded with a 4.4-fold increase (p=0.0001) in the fraction of *S*-palmitoylated NOD2 compared to DMSO in the acyl-RAC assay. In contrast, the THL treatment did not significantly impact the amount of palmitoylated NOD2 protein captured during the assay (p=0.3247) (Figure 2*C, D*).

These data suggest that one of the ABHD17 enzymes may be the main enzymes responsible for the depalmitoylation of NOD2.

Overexpression of ABHD17 enzymes depletes the plasmalemmal pool of NOD2

Having narrowed the list of candidate enzymes using inhibitors, we next examined the cellular consequences of expressing the individual α/β-hydrolases targeted by THL and ABD957. Preventing NOD2 *S*-palmitoylation by mutating Cys395 and Cys1033 or treating cells with 2-bromo-palmitate (2-BP) has been shown to prevent NOD2 from localizing to the PM [19,20]. We expected overexpressing an α/β-hydrolase enzyme capable of depalmitoylating NOD2 to similarly reduce the fraction of GFP-NOD2 associated with the PM. HCT116 cells stably expressing GFP-NOD2 were transiently transfected with individual isoforms (17A, 17B or 17C) (Figure S1*A*). We found that all three ABHD17 isoforms significantly redistributed GFP-NOD2 from PM to cytosol however, ABHD17B and 17C were the most effective in this assay (Figure S1*B*). In contrast, overexpression of the THL-sensitive ABHD6, ABHD12 and ABHD16A did not deplete the plasmalemmal GFP-NOD2 signal (Figure S1*C*, *D*). These data further support ABHD17 isoforms as the main NOD2 depalmitoylation enzymes.

ABHD17 knockdown increases the plasmalemmal enrichment of NOD2 and ligand-induced signaling

To determine if endogenous ABHD17 enzymes regulate NOD2 depalmitoylation in cells we investigated the effects of ABHD17 knockdown on NOD2 palmitoylation in HCT116 cells. Prior to this experiment, the relative expression of ABHD17 isoforms was

analyzed using quantitative polymerase chain reaction (qPCR). All three isoforms have similar levels of mRNA in HCT116 cells (Figure 3*A*), and thus we targeted all three isoforms. Reverse transcription (RT)-qPCR showed efficient silencing of ABHD17A, 17B and 17C either individually or in combination 48 hours after one round of siRNA transfections (Figure 3*B*). Silencing of ABHD17A had no significant effect on NOD2 localization (p= 0.1306) (Figure 3*C*, *D*) whereas knockdown of ABHD17B and ABHD17C each had a moderate effect on NOD2 membrane localization 1.8-fold (p=0.0007) and 1.6-fold (p=0.0203) increase, respectively. However, the simultaneous knockdown of all three ABHD17 isoforms resulted in a 3.9-fold increase (p<0.0001) in GFP-NOD2 associated with the PM. Furthermore, the triple knockdown (Triple KD) result was comparable to the selective ABHD17 inhibitor. Collectively, the results from overexpression and silencing experiments indicate that ABHD17B and C are the primary thioesterases responsible for NOD2 depalmitoylation in HCT116 cells and that ABHD17A may play less of a role or perhaps is more important in other cell types.

Next, we examined how inhibiting or silencing ABHD17 would affect endogenous NOD2-dependent activation and downstream pathways. To do this, we monitored the phosphorylation status of downstream effector proteins NF-κB (p65), IκB and MAPK (p38) in response to NOD2-RIPK2 activation (Figure 3*E*). Previous research has shown that inhibiting *S*-palmitoylation of NOD2 reduces NF-κB and MAPK activity in RAW267.4 and HCT116 cells stimulated with MDP [19]. To do this HCT116 cells were treated with siRNAs or ABD957 prior to stimulation with a synthetic NOD2 agonist, L18-MDP. As predicted in cells with attenuated ABHD17 and elevated NOD2 palmitoylation, cells displayed an increase in the activation of NF-κB and MAPK responses (Figure 3*F*,

G and *H*). We next extended this finding to determine if the enhanced signal transduction resulted in an increase in cytokine production and secretion. The results demonstrate that the knockdown of each individual isoform was insufficient to promote increased cytokine production. Silencing all three isoforms was necessary for an enhanced release of proinflammatory cytokines and chemokines, as captured by a high-sensitivity multiplex assay. Among these, was granulocyte-macrophage colony-stimulating factor (GM-CSF) (Figure 3*I*). Both RNA interference and the ABD957 inhibitor resulted in a 3.6-fold and 1.8-fold increase in GM-CSF secretion, respectively. Similar results were found for another pro-inflammatory cytokine, IL-8, which displayed a more than 3-fold increase in secreted levels ($p<0.0001$) (Figure 3*J*). Together, these results demonstrate that the loss of ABHD17 function increases the levels of palmitoylated NOD2, which subsequently enhances the activity of the NF-κB and MAPK signaling pathways regulating the production of proinflammatory cytokines.

Inhibiting ABHD17 enzymes restores localization and S-palmitoylation of CD-associated NOD2 variants

It was previously reported that several CD-associated NOD2 loss-of-function variants have reduced palmitoylation levels [19]. Targeted inhibition of ABHD17 enzymes could potentially increase the degree of palmitoylation of these mutants and improve signal transduction in response to MDP. First, we examined the 3020insC frameshift mutation that encodes a truncated NOD2 protein lacking the last 33 amino acids (L1007fs). This C-terminal truncation lacks one of the two required palmitoylation sites, and previous data demonstrated that the remaining Cys residue was poorly

palmitoylated [19]. However, whether this was due to inefficient *S*-palmitoylation or rapid depalmitoylation was unknown. Here we treated cells expressing L1007fs with ABD957 and found that there was no impact on the localization of the GFP signal, and it remained devoid of plasmalemmal signal (Figure 4*A*) suggesting that the protein is a poor substrate for zDHHC5. Next, we focused on three other hypo-palmitoylated mutants, L248R, R702W and A755V. Again, we used the Sleeping Beauty transposon system to create a stable transgenic cell line for each mutant using HCT116 and HEK293T cells. We used confocal microscopy to examine the effects of inhibitors (THL, ABD957 and Palmostatin B) and RNA interference on the subcellular localization of each variant (Figure 4*B*). As we observed with wildtype NOD2, inhibiting ABHD17 significantly increased the recruitment of L248R, R702W and A755V to the PM (Figure 4*C*-*E*). Contrary to what we observed with wildtype NOD2, THL had no significant impact on the localization of the NOD2 mutants ($p > 0.05$). We also observed an increase in *S*-palmitoylated protein captured using acyl-RAC, for variants treated with Palmostatin B and ABD957 (Figure 4*F*). Together, these results suggest that the hypo-palmitoylated NOD2 mutants are substrates for both the acyltransferase zDHHC5 and the thioesterases, ABHD17 enzymes. Notably, inhibiting the depalmitoylation mediated by the thioesterases increased their respective plasmalemmal localization.

Next, we examined how simply increasing the fraction associated with the PM influenced their ability to transduce signals. For this, we used Sleeping Beauty-engineered stable HEK293T cells with little to no endogenous NOD2 [7,38] as a model for exploring agonist-induced NF-κB activation and cytokine production. Protein expression was induced with 10 ng/mL doxycycline for 18-20h. We titrated doxycycline to the

lowest effective concentration to induce expression while preventing spurious activation of NOD2-mediated NF-κB signaling. Cells were stimulated with 100 ng/mL L18-MDP for 1h after RNA interference or 4h treatment with ABD957. We observed increased phosphorylation of IκB and p38 (Figure 4*G-I*), consistent with NOD2-RIPK2 activation of NF-κB and MAPK pathways as in the HCT116 cells. To correlate these acute stimulations with cytokine release from the cells, we again analyzed the supernatants for pro-inflammatory mediators IL-8 and TNFa. HEK293T cells stably expressing A755V exhibited significant ($p<0.0001$) 2.4 and 3.2-fold increases in IL-8 and TNFα secretions when cells were stimulated with L18-MDP (Figure 4*J*, *K*). Cells expressing R702W displayed a modest 1.5-fold increase ($p=0.0003$) in TNFα, and a 1.4-fold increase (not significant) in IL-8 secretions. Cells expressing L248R also displayed a modest, albeit not statistically significant, 2.4 and 1.3-fold increase in IL-8 and TNFα secretions when cells were stimulated with L18-MDP. Together, the results suggest that the hypo-palmitoylated NOD2 variants can be partly rescued by inhibiting ABHD17 enzymes.

DISCUSSION

The *S*-palmitoylation of NOD2 targets the protein to the PM, endosomes and phagosomes critical for MDP-induced signaling in response to bacterial infection [19]. Here, we demonstrate that ABHD17 enzymes remove the two acyl chains from NOD2 and thus negatively regulate NOD2-mediated NF-κB signaling. The results further highlight how the *S*-palmitoylation – depalmitoylation cycle is a pivotal regulator of NOD2 function and that hypo-palmitoylated variants can be improved by targeting the ABHD17 family of thioesterases. This study further supports the previous findings that

defective NOD2 *S*-palmitoylation renders the protein non-functional in response to MDP and may contribute to CD's pathogenesis. Our findings also raise the possibility that approaches that attenuate the depalmitoylation of NOD2 variants may be beneficial therapeutically.

In this study, we investigated NOD2 loss-of-function variants associated with CD, including two of the more prevalent NOD2 mutations, L1007fs and R702W. R702W is a missense mutation, whereas the L1007 frameshift results from an insertion of a C residue at position 3020 in the coding sequence. The c-terminal truncation of 1007fs deletes one of the two *S*-palmitoylation sites. Both these mutant proteins, in addition to L248R and A755V, are hypo-palmitoylated and mislocalized in cells and have lost the ability to induce NF-κB signaling in response to MDP [19] (Figure 4). Given the previous findings and the fact that one of the Cys residues is missing, we did not anticipate inhibiting ABHD17 would improve the localization and functionality of the L1007fs variant. However, we did observe improved *S*-palmitoylation, localization and functionality in the other three hypo-palmitoylated mutants. It remains unknown which among the sixty CD-associated NOD2 variants are hypo-palmitoylated. Nonetheless, targeted inhibition of ABHD17 could prove advantageous for a specific subset of these variants.

The connection between NOD2 loss-of-function mutants and CD may have significant implications for the disease. This is not only because dysfunction in the innate immune system is crucial in CD's development, but also because it has been demonstrated that restoring normal innate signaling can alleviate colitis [39]. However, ongoing debates exist regarding how changes in NOD2 signaling can increase

susceptibility to inflammation and the role post-transcriptional regulation plays in patients with or without NOD2 variants associated with the disease and their resulting pathogenic innate immune responses [40,41]. *S*-palmitoylation has been shown to impede autophagic degradation of NOD2 by attenuating binding to the cargo receptor p62/SQSTM1 [42]. The degradation rate is remarkably higher for *S*-palmitoylation-deficient NOD2 variants wild-type NOD2 [42,43]. Thus, ABHD17 enzymes may also regulate NOD2 stability by coupling depalmitoylation to selective autophagy. Finally, additional roles for NOD2 have been described in response to viruses and ER stress. As these roles for NOD2 do not require localization to the PM or endocytic organelles, it is currently unclear if they will require *S*-palmitoylated NOD2 or if ABHD17 isoforms will control these pathways. Indeed, it is tempting to speculate that the reason why both plasmalemmal (*S*-palmitoylated) and cytosolic (non-palmitoylated) pools of NOD2 exist is that it may allow it to function in many subcellular compartments under a variety of conditions.

ACKNOWLEDGEMENTS

The authors thank the Kennan Research Center for Biomedical Science Core Facilities at St. Michael's Hospital, especially Dr Caterina Di Ciano-Oliveira and Dr Monika Lodyga, for their continued support, technical advice, expertise, and training. This work was supported by a Project Grant from the Canadian Institutes of Health Research (grant no.: PJT166010; to G.D.F.), an Innovator Award from the Kenneth Rainin Foundation, and a grant from the National Institutes of Health, R01CA193994 to B.F.C. G.D.F. is supported by a Tier 1 Canada Research Chair in Multiomics of Lipids and

Innate Immunity. C.L.D. was supported by a Breakthrough Accelerator Fellowship from the Dalhousie Medical Research Foundation/Medical Research Development Office. The graphical abstract was created using BioRender.com.

AUTHOR CONTRIBUTIONS

C.L.D. and G.D.F. conceptualization; C.L.D methodology; C.L.D. formal analysis; C.L.D. and N.R.M. investigation; M.J.N and B.F.C resources; C.L.D and G.D.F. writing–original draft; C.L.D. and G.D.F. writing–review & editing; C.L.D. and G. D. F. visualization; G.D.F. supervision; G.D.F. project administration; B.F.C and G. D. F. funding acquisition.

DECLARATION OF INTERESTS

The authors declare that the research was conducted in the absence of any commercial or financial relationships that could be construed as a potential conflict of interest.

INCLUSION AND DIVERSITY

We support inclusive, diverse, and equitable conduct of research. Dalhousie University is located in Mi'kma'ki, the ancestral and unceded territory of the Mi'kmaq.

STAR Methods

KEY RESOURCES TABLE

REAGENT or RESOURCE	SOURCE	IDENTIFIER
Antibodies		
Mouse monoclonal anti-GFP	Cell Signaling Technologies	Cat#2955S
Mouse monoclonal anti-GAPDH	Cell Signaling Technologies	Cat#97166S; Lot#6

Rabbit monoclonal phospho-NF-κB p65	Cell Signaling Technologies	Cat#3033S; Lot#19
Rabbit monoclonal NF-κB p65	Cell Signaling Technologies	Cat#8242S; Lot#16
Rabbit polyclonal phospho-p38 MAPK	Cell Signaling Technologies	Cat#9211S; Lot#27
Rabbit polyclonal p38 MAPK	Cell Signaling Technologies	Cat#9212S; Lot#26
Mouse monoclonal phospho-IκBα	Cell Signaling Technologies	Cat#9246S; Lot#23
Mouse monoclonal anti-HA	Cell Signaling Technologies	Cat#2367S; Lot#5
Goat anti-Rabbit horseradish peroxidase	Cell Signaling Technologies	Cat#7074S; Lot#32
Goat anti-Mouse horseradish peroxidase	Cell Signaling Technologies	Cat#7076S; Lot#38
Mouse monoclonal anti-NOD2 (clone 2D9)	Invitrogen	Cat#MA1-16611; Lot#3959536
Cy5-conjugated Goat anti-Mouse IgG	Jackson ImmunoResearch	Cat#115-175-166
Bacterial and virus strains		
Biological samples		
Chemicals, peptides, and recombinant proteins		
L18-MDP	Invitrogen	Cat#tlrl-lmdp
ML348	Sigma-Aldrich	Cat#899713-86-1
ML349	Sigma-Aldrich	Cat#890819-86-0
WWL70	Sigma-Aldrich	Cat#947669-91-2
Orlistat	Sigma-Aldrich	Cat#96829-58-2
S-Methyl thiomethanesulfonate	Sigma-Aldrich	Cat#64306
Hydroxylamine	Sigma-Aldrich	Cat#159417
4',6-diamidine-2'-phenylindole dihydrochloride	Sigma-Aldrich	Cat#10236276001
NP-40	Sigma-Aldrich	Cat#492016-500L
Triton X-100	Sigma-Aldrich	Cat#X-100
Puromycin	Sigma-Aldrich	Cat#P4512
Palmostatin B	EMD Millipore	Cat#178501
RIPA	EMD Millipore	Cat#20-188
Doxycycline Hydrochloride	Bio Basic Inc.	Cat#DB0889
Dulbecco's Modification of Eagle's Medium	Wisent Inc.	Cat#319-020-CL
Fetal Bovine Serum	Wisent Inc.	Cat#080150
ViaFect Transfection Reagent	Promega	Cat# E498A
DharmaFECT2	Horizon Discovery Biosciences	Cat#T-2002-02; Lot#
ABD957	Benjamin Cravatt Lab, The Scripps Research Institute; Remsberg et al.[37]	
Phosphate Buffered Saline	Wisent Inc.	Cat#311-010-CL
PhosSTOP Phosphatase Inhibitor	Roche	Cat#04906845001
EDTA-free Protease Inhibitor	BioShop	Cat#PIC002-1

SlowFade Glass Antifade Mountant	ThermoFisher Scientific	Cat#S36918; Lot#2142092
NucBlue Fixed Cell ReadyProbes Reagent	Invitrogen	Cat#R37606
Critical commercial assays		
High-Capacity Acyl-RAC S3 Capture Beads	NANOCS	Cat#AR-S3-1
QuikChange II XL Site-Directed Mutagenesis Kit	Agilent	Cat #200521
No-Stain Protein Labeling Reagent	ThermoFisher Scientific	Cat#A44449
Pierce BCA Protein Assay Kit	ThermoFisher Scientific	Cat#23225
NucleoSpin RNA Purification Kit	Macherey-Nagel	Cat#740955.50
SensiFAST cDNA Synthesis Kit	FroggaBio	Cat#65053
Deposited data		
Experimental models: Cell lines		
Human: Colorectal Carcinoma HCT 116	ATCC	CCL-247
Human: Embryonic Kidney (HEK) 293T	ATCC	CRL-3216
Experimental models: Organisms/strains		
Oligonucleotides		
siRNA targeting sequence: ON-TARGETplus Human ABHD17A: ACGUGAAAACGGAAAUUAA	Horizon Discovery Biosciences	Cat# J-005947-12-0020; Lot#211109
siRNA targeting sequence: ON-TARGETplus SMARTpool Human ABHD17B: GGACUAGGAUCACGGAUUA, GGAUCUUGCUGCUCGAUAU, GUUCACCCAAUGCGAAAUA, UCGCAUUGUUUGAACGUUG	Horizon Discovery Biosciences	Cat# L-005809-01-0020; Lot#211112
siRNA targeting sequence: ON-TARGETplus Human ABHD17C: CCACCAAUGUUCUCGGUAU	Horizon Discovery Biosciences	Cat# J-005929-10-0020; Lot#211109
siRNA targeting sequence: ON-TARGETplus Non-Targeting: UGGUUUACAUGUCGACUAA	Horizon Discovery Biosciences	Cat# D-001810-01-20
Primers for RT-qPCR, See Table S1	This paper	N/A
Recombinant DNA		
Plasmid: pEF-BOS-HA	Gift from Dr. Jennifer Greaves, Coventry University; Fukata et al.[44]	
Plasmid: pEF-BOS-HA-ABHD17A	Gift from Dr. Jennifer Greaves, Coventry University	N/A
Plasmid: pEF-BOS-HA-ABHD17B	Gift from Dr. Jennifer Greaves, Coventry University	N/A
Plasmid: pEF-BOS-HA-ABHD17C	Gift from Dr. Jennifer Greaves, Coventry University	N/A
Plasmid: pEF-BOS-HA-ABHD6	Gift from Dr. Jennifer Greaves, Coventry University	N/A

Plasmid: pEF-BOS-HA-ABHD12	Gift from Dr. Jennifer Greaves, Coventry University; Ahonen et al.[45]	N/A
Plasmid: pEF-BOS-HA-ABHD16A	Gift from Dr. Jennifer Greaves, Coventry University; Ahonen et al.[45]	N/A
Plasmid pSBtet-BP	Kowarz et al.[46]	Addgene Plasmid #60496
Plasmid: pCMV(CAT)T7-SB100	Mátés et al.[47]	Addgene Plasmid #34879
Plasmid: pSB-GFP-NOD2	This paper	
Plasmid: pSB-GFP-NOD2 L248R	This paper	
Plasmid: pSB-GFP-NOD2 R702W	This paper	
Plasmid: pSB-GFP-NOD2 A755V	This paper	
Software and algorithms		
ImageJ2 v2.14.0/1.54f	Rueden et al.[48]	
Other		

RESOURCE AVAILABILITY

Lead contact

Further information and requests for resources and reagents should be directed to and will be fulfilled by the lead contact, Gregory Fairn (gfairn@dal.ca)

Materials availability

- Any plasmids or cell lines generated in this study are available upon request.

Data and code availability

- Original western blot images have been deposited at Zenodo and are publicly available as of the date of publication at [insert DOI]. The lead contact will share the Microscopy data reported in this paper upon request.
- This paper does not report any original code.
- Any additional information required to reanalyze the data reported in this paper is available from the lead contact upon request.

EXPERIMENTAL MODEL AND STUDY PARTICIPANT DETAILS

Immortalized and engineered cell lines

Cells were purchased from the American Type Culture Collection (ATCC). Human colorectal carcinoma HCT116 and human embryonic kidney (HEK) 293T cell lines were maintained and propagated in high glucose Dulbecco's modification of Eagle's medium (DMEM) from Wisent (St. Bruno, Canada, cat# 319-020-CL) supplemented with 1.5 g/L sodium bicarbonate, L-glutamine and 10% fetal bovine serum (Wisent, cat# 080150) in a humidified incubator at 37 °C, 5% CO_2.

Stable cells were generated using the sleeping beauty transposon system [46]. To generate doxycycline-inducible stable integration of GFP-NOD2, cells were co-transfected with sleeping beauty vector (pSBTet-BP [46], Addgene # 60496) carrying the gene of interest and small amounts of the transposase encoding plasmid, pCMV(CAT)T7-SB100 [47] (Addgene # 34879). Cells were transfected using ViaFect transfection reagent (Promega, Madison, WI) according to the manufacturer's instructions. Forty-eight hours after transfection, cells were selected for puromycin resistance over 3-5 days and terminated when virtually all the cells displayed the expected doxycycline inducible GFP or constitutive BFP fluorescence. Expression of the GFP-NOD2 and the indicated mutants was induced using 1 µg/mL doxycycline unless otherwise indicated. Stable expression of GFP chimeric proteins was confirmed using microscopy and immunoblotting.

METHOD DETAILS

Transfections

cDNA transfections were performed using Promega ViaFect (cat# E4982), while siRNA transfections were performed using DharmaFECT2 (cat# T-2002-02) purchased from Horizon Discovery Biosciences. HCT116 cells were transfected with cDNAs as indicated in each experiment using ViaFect as per manufacturer's instructions. For immunofluorescence studies, HCT116 cells were grown on glass coverslips in 12-well plates and transfected at 60–80% confluence with 1 μg of cDNA per well for each of the indicated thioesterase encoding plasmids using Promega's Viafect according to product instructions.

Unless otherwise stated, for RNA interference experiments two rounds of transfection were used to introduce 100nM small interfering RNA in HCT116 and HEK293T on days 1 and 2 post-plating. For knockdown experiments, the ON-TARGETplus siRNA of targeted genes and the non-targeting siRNA were purchased from Horizon Discovery Biosciences. The silencer siRNA used are as follows: ON-TARGETplus Non-targeting siRNA, 5'-UGGUUUACAUGUCGACUAA- 3', ON-TARGETplus Human ABHD17A siRNA, 5'-ACGUGAAAACGGAAAUUAA-3', ON-TARGETplus Human ABHD17C siRNA, 5'-CCACCAAUGUUCUCGGUAU-3', ON-TARGETplus SMARTpool Human ABHD17B siRNA (1# 5'-GGACUAGGAUCACGGAUUA-3', 2# 5'-GGAUCUUGCUGCUCGAUAU-3', 3# 5'-GUUCACCCAAUGCGAAAUA-3', 4# 5'-UCGCAUUGUUUGAACGUUG-3'). Since isoform-specific antibodies against ABHD17 isoforms are not available, RT-qPCR was used to quantify the degree of mRNA knockdown.

Experimentally cells transfected with siRNA were induced with doxycycline on day 3, followed by confocal microscopy, cell were stimulated with L18-MDP on day 4, 18-20h following induction.

Inhibitor assays

Stable transfected HCT116 were cultured as monolayers on 18mm round glass coverslips in 12-well plates. Stable expression of GFP-tagged NOD2 or NOD2 variant was induced with doxycycline (1 µg/mL). Approximately 18-20h after induction, cells were treated with DMSO vehicle (control) or small molecule inhibitors Palmostatin B, Orlistat (tetrahydrolipstatin; THL), ABD957, WWL70, ML348, ML349 for 4 h at 37°C in 5% CO_2.

Preparation of cell extracts

Stable transfected HCT116 and HEK293T cells were induced with doxycycline (1 µg/mL) for 18-20 h, then treated with inhibitors or stimulated as indicated. Cells were harvested in phosphate-buffered saline (D-PBS; cat# 311-010-CL) from Wisent Inc., and lysed in RIPA buffer (CST; cat# 9806S) or NP-40 lysis buffer containing PhosSTOP phosphatase inhibitor (Roche; cat# 04906845001) and EDTA-free protease inhibitor (BioShop; cat# PIC002-1) and incubated on ice for 1 hour, then centrifuged at 10,000 x*g* at 4°C for 10 minutes to obtain clear lysates. Protein concentration was determined with Pierce BCA protein assay (Thermo Scientific; cat# 23225).

Confocal microscopy

Cells were seeded on 18 mm-round glass coverslips in 12-well plates. Stable HCT116 cells expressing GFP-NOD2 wildtype and mutants were washed with PBS and fixed with a 4% paraformaldehyde solution for 20 min at room temperature. Glass coverslips were washed with PBS then incubated with 100 mM glycine, 0.1% v/v Triton X-100 for 20 min at room temperature. Cells were blocked with 5% BSA in PBS for 1h at room temperature and then probed with 1:100 anti-HA (CST) antibody overnight. The coverslips were washed three times with PBS, followed by a 1h incubation with species-matched 1:500 Cy5-conjugated goat anti-mouse IgG (Jackson ImmunoResearch) in PBS. Images were acquired in the St. Michael's Hospital Bioimaging Facility using a Zeiss Axiovert 200M microscope equipped with a Yokogawa CSU-X1 confocal spinning disc system and a 63X Apo PLAN VC, NA 1.40 oil objective and a Hamamatsu ImagEM X2 EM-CCD camera. Images were processed using ImageJ2 version 2.14.0/1.54f.

Acyl resin-assisted-capture (Acyl-RAC)

Stable HCT116 cells were harvested and lysed (1% Triton X-100, 50 mM Tris-HCl (pH 7.5), 150 mM NaCl, 1 mM EDTA, 1 % SDS, 0.5 % sodium deoxycholate, 1X protease inhibitor (BioShop; cat# PIC002-1), 0.2% v/v methyl methanethiosulfonate (MMTS). Lysates were sonicated and incubated at 42°C in a thermal shaker for 3h. Blocking was stopped, and MMTS was removed with 3-4 rounds of methanol/chloroform precipitation. The protein pellets were rinsed with methanol and air-dried. The pellets were redissolved in binding buffer (100 mM Tris- HCl (pH 7.5), 1 mM EDTA, 1 % SDS) by incubating at 42°C in a thermal shaker, with intermittent mixing. The samples were sonicated in a water bath for 5-10 min to resuspend any undissolved pellet further. Each

sample was divided in two, and 50 µL of hydroxylamine (NH_2OH, 400 mM final concentration; or NaCl for control samples) was added before incubation with 25 µL of packed acyl-RAC beads (High-Capacity Acyl-RAC S3 beads; Nanocs # AR-S3-1,2) for 2 h at room temperature. The beads were washed 3 times with binding buffer before adding 4X SDS sample buffer with DTT and incubating the slurry at 80°C for 15 minutes.

RNA extraction and RT-qPCR

Total RNA was extracted from HCT116 cells Macherey-Nagel NucleoSpin RNA purification kit (cat# 740955.50; Allentown, PA) according to the manufacturer's protocols. cDNA was synthesized from 1 µg RNA using SensiFAST cDNA Synthesis Kit (FroggaBio; Concord, Canada). qPCR was performed using a QuantStudio™ 7 Flex Real-Time PCR System in conjunction with a SybrGreen System (Thermo Scientific; Oakville, Canada). All cycle threshold (C_T) values were normalized to GAPDH. The relative expression level for each gene of interest was calculated using the $2^{-\Delta\Delta C_T}$ method [49]. The primer sequences were as follows: Human *ABHD17A* forward: 5'-ACCATCGAGGTCTTCCCCACCAGG-3', Human *ABHD17A* reverse: 5'-AGAAGAGGACCGTGTACCTGGCACC-3', Human *ABHD17B* forward: 5'-CCGCTCAGGTGCAGAGCATGAATAA-3', Human *ABHD17B* reverse: 5'-AAGCAATCTTCCCTGGACAAGGTGG-3', Human *ABHD17C* forward: 5'-TTGATGCTTTCCCCAGCATTGACA-3', Human *ABHD17C* reverse: 5'-TCGCTAGGCCATGGGAGAAATCG-3', Human *GAPDH* forward: 5'-

CAATGACCCCTTCATTGACC-3', Human *GAPDH* reverse: 5'-GACAAGCTTCCCGTTCTCAG-3'.

Multiplex analysis of secreted cytokines

Using 12 well tissue culture plates, cells were cultured with DMEM containing 10% FBS. Cells were treated with siRNA complexes over 48 hours or ABD957 inhibitor for 4 hours, before brief stimulation with 100 ng/mL L18-MDP (1h for HEK293T cells and 6h for HCT116 cells). Plates were maintained at 37 °C in 5% CO_2 for 24 h. Next, supernatants were collected and analyzed using Luminex-100 MAP® technology for a panel of 14 human cytokines, chemokines, and growth factors. Specifically, plates were placed on ice, the contents of the wells for each condition (unstimulated, L18-MDP-stimulated) were transferred to 1.5mL microcentrifuge tubes, and samples were centrifuged at 4 °C for 10 min at 11,000 × *g* followed by distribution of the supernatant into 200 µl aliquots that were immediately frozen at −80 °C and maintained frozen until analysis. This was repeated 3 times to obtain 3 independent replicates. This multiplexing analysis was performed using a Luminex™ 200 system (Luminex, Austin, TX, USA) by Eve Technologies Corp. (Calgary, Alberta). Fourteen markers were simultaneously measured in the samples using Eve Technologies' Human High Sensitivity 14-Plex Discovery Assay® (MilliporeSigma, Burlington, Massachusetts, USA). The 14-plex consisted of GM-CSF, IFNγ, IL-1β, IL-2, IL-4, IL-5, IL-6, IL-8, IL-10, IL-12p70, IL-13, IL-17A, IL-23, TNF-α. Assay sensitivities of these markers range from 0.11 – 3.25 pg/mL for the 14-plex, and some samples required dilution for accurate determination. Individual analyte sensitivity values are available in the MilliporeSigma

MILLIPLEX® MAP protocol. Only molecules that reached the low end of the sensitivity are depicted in the results.

QUANTIFICATION AND STATISTICAL ANALYSIS

Statistical differences ($p < 0.05$) were inferred using Student's two-tailed t-tests or one-way ANOVA with Dunnett's correction or two-way ANOVA with Fisher's least significant difference (LSD) method for multiple comparisons performed using Prism 10 (Graph-Pad Software, Inc., La Jolla, CA) with DMSO-treated, vector-co-transfected, or non-targeting siRNA-transfected samples as the control group. All significant differences are indicated in the text and figures. The statistical significance threshold was set to 0.05 throughout this study.

Cell membrane fluorescence intensity and immunoblot band intensities were quantified using ImageJ2 open-source image processing software.

REFERENCES

1. Hugot, J.P., Chamaillard, M., Zouali, H., Lesage, S., Cézard, J.P., Belaiche, J., Almer, S., Tysk, C., O'Morain, C.A., Gassull, M., et al. (2001). Association of NOD2 leucine-rich repeat variants with susceptibility to Crohn's disease. Nature *411*, 599-603. 10.1038/35079107.
2. Ogura, Y., Bonen, D.K., Inohara, N., Nicolae, D.L., Chen, F.F., Ramos, R., Britton, H., Moran, T., Karaliuskas, R., Duerr, R.H., et al. (2001). A frameshift mutation in NOD2 associated with susceptibility to Crohn's disease. Nature *411*, 603-606. 10.1038/35079114.
3. Hampe, J., Cuthbert, A., Croucher, P.J., Mirza, M.M., Mascheretti, S., Fisher, S., Frenzel, H., King, K., Hasselmeyer, A., Macpherson, A.J., et al. (2001). Association between insertion mutation in NOD2 gene and Crohn's disease in German and British populations. The Lancet *357*, 1925-1928. 10.1016/s0140-6736(00)05063-7.
4. Franchi, L., Warner, N., Viani, K., and Nuñez, G. (2009). Function of Nod-like receptors in microbial recognition and host defense. Immunological Reviews *227*, 106-128. 10.1111/j.1600-065x.2008.00734.x.
5. Ricardo, Milutinovic, S., and John (2012). Roles of NOD1 (NLRC1) and NOD2 (NLRC2) in innate immunity and inflammatory diseases. Bioscience Reports *32*, 597-608. 10.1042/bsr20120055.
6. Caruso, R., Warner, N., Inohara, N., and Núñez, G. (2014). NOD1 and NOD2: Signaling, Host Defense, and Inflammatory Disease. Immunity *41*, 898-908. 10.1016/j.immuni.2014.12.010.
7. Ogura, Y., Inohara, N., Benito, A., Chen, F.F., Yamaoka, S., and Núñez, G. (2001). Nod2, a Nod1/Apaf-1 Family Member That Is Restricted to Monocytes and Activates NF-κB. Journal of Biological Chemistry *276*, 4812-4818. 10.1074/jbc.m008072200.
8. Keestra, A.M., and Bäumler, A.J. (2014). Detection of enteric pathogens by the nodosome. Trends in Immunology *35*, 123-130. 10.1016/j.it.2013.10.009.
9. Moreira, L.O., and Zamboni, D.S. (2012). NOD1 and NOD2 Signaling in Infection and Inflammation. Frontiers in Immunology *3*. 10.3389/fimmu.2012.00328.
10. Voss, E., Wehkamp, J., Wehkamp, K., Stange, E.F., Schröder, J.M., and Harder, J. (2006). NOD2/CARD15 mediates induction of the antimicrobial peptide human beta-defensin-2. J Biol Chem *281*, 2005-2011. 10.1074/jbc.M511044200.
11. Grimm, M.C., and Pavli, P. (2004). NOD2 mutations and Crohn's disease: are Paneth cells and their antimicrobial peptides the link? Gut *53*, 1558-1560. 10.1136/gut.2004.043307.
12. Homer, C.R., Richmond, A.L., Rebert, N.A., Achkar, J.P., and McDonald, C. (2010). ATG16L1 and NOD2 interact in an autophagy-dependent antibacterial pathway implicated in Crohn's disease pathogenesis. Gastroenterology *139*, 1630-1641, 1641.e1631-1632. 10.1053/j.gastro.2010.07.006.
13. Hampe, J., Franke, A., Rosenstiel, P., Till, A., Teuber, M., Huse, K., Albrecht, M., Mayr, G., De La Vega, F.M., Briggs, J., et al. (2007). A genome-wide association scan of nonsynonymous SNPs identifies a susceptibility variant for Crohn disease in ATG16L1. Nat Genet *39*, 207-211. 10.1038/ng1954.

14. Travassos, L.H., Carneiro, L.A., Ramjeet, M., Hussey, S., Kim, Y.G., Magalhães, J.G., Yuan, L., Soares, F., Chea, E., Le Bourhis, L., et al. (2010). Nod1 and Nod2 direct autophagy by recruiting ATG16L1 to the plasma membrane at the site of bacterial entry. Nat Immunol *11*, 55-62. 10.1038/ni.1823.
15. Gutierrez, O., Pipaon, C., Inohara, N., Fontalba, A., Ogura, Y., Prosper, F., Nunez, G., and Fernandez-Luna, J.L. (2002). Induction of Nod2 in myelomonocytic and intestinal epithelial cells via nuclear factor-kappa B activation. J Biol Chem *277*, 41701-41705. 10.1074/jbc.M206473200.
16. Charrière, G.M., Ip, W.E., Dejardin, S., Boyer, L., Sokolovska, A., Cappillino, M.P., Cherayil, B.J., Podolsky, D.K., Kobayashi, K.S., Silverman, N., et al. (2010). Identification of Drosophila Yin and PEPT2 as evolutionarily conserved phagosome-associated muramyl dipeptide transporters. J Biol Chem *285*, 20147-20154. 10.1074/jbc.M110.115584.
17. Nakamura, N., Lill, J.R., Phung, Q., Jiang, Z., Bakalarski, C., De Mazière, A., Klumperman, J., Schlatter, M., Delamarre, L., and Mellman, I. (2014). Endosomes are specialized platforms for bacterial sensing and NOD2 signalling. Nature *509*, 240-244. 10.1038/nature13133.
18. Kim, Y.G., Kamada, N., Shaw, M.H., Warner, N., Chen, G.Y., Franchi, L., and Núñez, G. (2011). The Nod2 sensor promotes intestinal pathogen eradication via the chemokine CCL2-dependent recruitment of inflammatory monocytes. Immunity *34*, 769-780. 10.1016/j.immuni.2011.04.013.
19. Lu, Y., Zheng, Y., Coyaud, É., Zhang, C., Selvabaskaran, A., Yu, Y., Xu, Z., Weng, X., Chen, J.S., Meng, Y., et al. (2019). Palmitoylation of NOD1 and NOD2 is required for bacterial sensing. Science *366*, 7.
20. Dixon, C.L., and Fairn, G.D. (2021). S-palmitoylation of NOD2 controls its localization to the plasma membrane. Journal of Lipid Research, 100097. 10.1016/j.jlr.2021.100097.
21. Guan, X., and Fierke, C.A. (2011). Understanding Protein Palmitoylation: Biological Significance and Enzymology. Sci China Chem *54*, 1888-1897. 10.1007/s11426-011-4428-2.
22. Morrison, E., Wegner, T., Zucchetti, A.E., Álvaro-Benito, M., Zheng, A., Kliche, S., Krause, E., Brügger, B., Hivroz, C., and Freund, C. (2020). Dynamic palmitoylation events following T-cell receptor signaling. Communications Biology *3*. 10.1038/s42003-020-1063-5.
23. He, Y., and Linder, M.E. (2008). Differential palmitoylation of the endosomal SNAREs syntaxin 7 and syntaxin 8. *50*, 398-404. 10.1194/jlr.m800360-jlr200.
24. Lynch, S.J., Snitkin, H., Gumper, I., Philips, M.R., Sabatini, D., and Pellicer, A. (2015). The Differential Palmitoylation States of N-Ras and H-Ras Determine Their Distinct Golgi Subcompartment Localizations. *230*, 610-619. 10.1002/jcp.24779.
25. Barnich, N., Aguirre, J.E., Reinecker, H.-C., Xavier, R., and Podolsky, D.K. (2005). Membrane recruitment of NOD2 in intestinal epithelial cells is essential for nuclear factor–κB activation in muramyl dipeptide recognition. Journal of Cell Biology *170*, 21-26. 10.1083/jcb.200502153.

26. Lé, Cine, P., Esmiol, S., Mé, Tais, J.-Y., Nicoletti, C., Nourry, C., McDonald, C., Nunez, G., Hugot, J.-P., et al. (2007). The NOD2-RICK Complex Signals from the Plasma Membrane. Journal of Biological Chemistry *282*, 15197-15207. 10.1074/jbc.m606242200.
27. Dekker, F.J., Rocks, O., Vartak, N., Menninger, S., Hedberg, C., Balamurugan, R., Wetzel, S., Renner, S., Gerauer, M., Schölermann, B., et al. (2010). Small-molecule inhibition of APT1 affects Ras localization and signaling. Nature Chemical Biology *6*, 449-456. 10.1038/nchembio.362.
28. Rusch, M., Zimmermann, T.J., Bürger, M., Dekker, F.J., Görmer, K., Triola, G., Brockmeyer, A., Janning, P., Böttcher, T., Sieber, S.A., et al. (2011). Identification of acyl protein thioesterases 1 and 2 as the cellular targets of the Ras-signaling modulators palmostatin B and M. Angew Chem Int Ed Engl *50*, 9838-9842. 10.1002/anie.201102967.
29. Lin, D.T.S., and Conibear, E. (2015). ABHD17 proteins are novel protein depalmitoylases that regulate N-Ras palmitate turnover and subcellular localization. eLife *4*. 10.7554/elife.11306.
30. Cao, Y., Qiu, T., Kathayat, R.S., Azizi, S.A., Thorne, A.K., Ahn, D., Fukata, Y., Fukata, M., Rice, P.A., and Dickinson, B.C. (2019). ABHD10 is an S-depalmitoylase affecting redox homeostasis through peroxiredoxin-5. Nat Chem Biol *15*, 1232-1240. 10.1038/s41589-019-0399-y.
31. Bononi, G., Tuccinardi, T., Rizzolio, F., and Granchi, C. (2021). α/β-Hydrolase Domain (ABHD) Inhibitors as New Potential Therapeutic Options against Lipid-Related Diseases. Journal of Medicinal Chemistry *64*, 9759-9785. 10.1021/acs.jmedchem.1c00624.
32. Savinainen, J.R., Patel, J.Z., Parkkari, T., Navia-Paldanius, D., Marjamaa, J.J., Laitinen, T., Nevalainen, T., and Laitinen, J.T. (2014). Biochemical and pharmacological characterization of the human lymphocyte antigen B-associated transcript 5 (BAT5/ABHD16A). PLoS One *9*, e109869. 10.1371/journal.pone.0109869.
33. Won, S.J., Davda, D., Labby, K.J., Hwang, S.Y., Pricer, R., Majmudar, J.D., Armacost, K.A., Rodriguez, L.A., Rodriguez, C.L., Chong, F.S., et al. (2016). Molecular Mechanism for Isoform-Selective Inhibition of Acyl Protein Thioesterases 1 and 2 (APT1 and APT2). ACS Chemical Biology *11*, 3374-3382. 10.1021/acschembio.6b00720.
34. Li, W., Blankman, J.L., and Cravatt, B.F. (2007). A functional proteomic strategy to discover inhibitors for uncharacterized hydrolases. J Am Chem Soc *129*, 9594-9595. 10.1021/ja073650c.
35. Navia-Paldanius, D., Savinainen, J.R., and Laitinen, J.T. (2012). Biochemical and pharmacological characterization of human α/β-hydrolase domain containing 6 (ABHD6) and 12 (ABHD12). J Lipid Res *53*, 2413-2424. 10.1194/jlr.M030411.
36. Kamat, S.S., Camara, K., Parsons, W.H., Chen, D.H., Dix, M.M., Bird, T.D., Howell, A.R., and Cravatt, B.F. (2015). Immunomodulatory lysophosphatidylserines are regulated by ABHD16A and ABHD12 interplay. Nat Chem Biol *11*, 164-171. 10.1038/nchembio.1721.
37. Remsberg, J.R., Suciu, R.M., Zambetti, N.A., Hanigan, T.W., Firestone, A.J., Inguva, A., Long, A., Ngo, N., Lum, K.M., Henry, C.L., et al. (2021). ABHD17 regulation of plasma membrane palmitoylation and N-Ras-dependent cancer growth. Nature Chemical Biology *17*, 856-864. 10.1038/s41589-021-00785-8.
38. Weichart, D., Gobom, J., Klopfleisch, S., Häsler, R., Gustavsson, N., Billmann, S., Lehrach, H., Seegert, D., Schreiber, S., and Rosenstiel, P. (2006). Analysis of NOD2-mediated

Proteome Response to Muramyl Dipeptide in HEK293 Cells. Journal of Biological Chemistry *281*, 2380-2389. 10.1074/jbc.m505986200.

39. Watanabe, T., Asano, N., Murray, P.J., Ozato, K., Tailor, P., Fuss, I.J., Kitani, A., and Strober, W. (2008). Muramyl dipeptide activation of nucleotide-binding oligomerization domain 2 protects mice from experimental colitis. J Clin Invest *118*, 545-559. 10.1172/jci33145.
40. Strober, W., Asano, N., Fuss, I., Kitani, A., and Watanabe, T. (2014). Cellular and molecular mechanisms underlying NOD2 risk-associated polymorphisms in Crohn's disease. Immunol Rev *260*, 249-260. 10.1111/imr.12193.
41. Salem, M., Seidelin, J.B., Rogler, G., and Nielsen, O.H. (2013). Muramyl dipeptide responsive pathways in Crohn's disease: from NOD2 and beyond. Cell Mol Life Sci *70*, 3391-3404. 10.1007/s00018-012-1246-4.
42. Zhou, L., Zeng, H., Cui, J., and Jin, S. (2022). Palmitoylation facilitates inflammation through suppressing NOD2 degradation mediated by the selective autophagy receptor SQSTM1. Autophagy *18*, 2254-2255. 10.1080/15548627.2022.2054041.
43. Zhou, L., He, X., Wang, L., Wei, P., Cai, Z., Zhang, S., Jin, S., Zeng, H., and Cui, J. (2022). Palmitoylation restricts SQSTM1/p62-mediated autophagic degradation of NOD2 to modulate inflammation. Cell Death & Differentiation. 10.1038/s41418-022-00942-z.
44. Fukata, M., Fukata, Y., Adesnik, H., Nicoll, R.A., and Bredt, D.S. (2004). Identification of PSD-95 Palmitoylating Enzymes. Neuron *44*, 987-996. 10.1016/j.neuron.2004.12.005.
45. Ahonen, T.J., Ng, C.P., Farinha, B., Almeida, B., Victor, B.L., Reynolds, C., Kalso, E., Yli-Kauhaluoma, J., Greaves, J., and Moreira, V.M. (2023). Probing the Interactions of Thiazole Abietane Inhibitors with the Human Serine Hydrolases ABHD16A and ABHD12. ACS Med Chem Lett *14*, 1404-1410. 10.1021/acsmedchemlett.3c00313.
46. Kowarz, E., Löscher, D., and Marschalek, R. (2015). Optimized Sleeping Beauty transposons rapidly generate stable transgenic cell lines. Biotechnology Journal *10*, 647-653. 10.1002/biot.201400821.
47. Mátés, L., Chuah, M.K., Belay, E., Jerchow, B., Manoj, N., Acosta-Sanchez, A., Grzela, D.P., Schmitt, A., Becker, K., Matrai, J., et al. (2009). Molecular evolution of a novel hyperactive Sleeping Beauty transposase enables robust stable gene transfer in vertebrates. Nat Genet *41*, 753-761. 10.1038/ng.343.
48. Rueden, C.T., Schindelin, J., Hiner, M.C., DeZonia, B.E., Walter, A.E., Arena, E.T., and Eliceiri, K.W. (2017). ImageJ2: ImageJ for the next generation of scientific image data. BMC Bioinformatics *18*, 529. 10.1186/s12859-017-1934-z.
49. Livak, K.J., and Schmittgen, T.D. (2001). Analysis of relative gene expression data using real-time quantitative PCR and the 2(-Delta Delta C(T)) Method. Methods *25*, 402-408. 10.1006/meth.2001.1262.

FIGURE LEGENDS

Figure 1. Inhibiting protein depalmitoylases alters NOD2 subcellular localization and *S*-acylation (A) Immunoblot showing doxycycline-inducible expression of GFP-NOD2. Equal loading of proteins was normalized with GAPDH. Scale bar, 100µm. **(B)** Fluorescent microscopy images (20X magnification) demonstrating GFP-NOD2 expression in cells cultured with 1 µg/mL doxycycline for 18 h. **(C)** Fluorescence microscopy of human colorectal carcinoma (HCT116) cells expressing stably transfected GFP-NOD2 (pseudo-colored in cyan). Cells were treated with 100µM palmostatin B (PalmB) or dimethyl sulfoxide (DMSO, vehicle) for 4 h. Scale bars, 5µm. **(D)** Quantification of PalmB treatment effect on GFP-NOD2 plasma membrane localization from images as in (D). **(E)** *S*-palmitoylation levels of GFP-NOD2 expressed in HCT116 cells in the presence of hydroxylamine (NH_2OH) or PalmB. *S*-acylated GFP-NOD2 was detected in total cell lysates using acyl resin-assisted-capture (acyl-RAC) assay and immunoblot analysis. **(F)** Quantification of *S*-acylation based on immunoblots as in (E). All data are representative of at least three independent experiments, and p-values for data in (D) and (F) were determined by paired two-tailed Student's t-test; $p \leq 0.05$ (*) and $p \leq 0.01$ (**).

Figure 2. Depalmitoylation of NOD2 is enzymatically mediated by ABHD17 family of enzymes (A) Confocal images showing localization of GFP-NOD2 (cyan) in HCT116 cells treated with selective small molecule acyl thioesterase inhibitors: 40 µM orlistatin (THL), 2.5 µM ABD957, 25 µM WWL70, 50 µM ML348 or 40 µM ML349 for 4 h. Scale bars, 5µm. (**B**) Quantification of GFP-NOD2 plasma membrane localization from images

as in (A). **(C)** *S*-acylation levels of GFP-NOD2 in HCT116 cells treated with THL, ABD957 or palmostatin B, were determined using acyl-RAC and immunoblot analysis. **(D)** Quantification of *S*-acylation based on immunoblots as in (G). All data are representative of at least three independent experiments. Statistical significance was determined by two-tailed Student's paired *t*-test or one-way ANOVA followed by Dunnett's post hoc test. Group differences were considered significant for $p \leq 0.05$ (*) and $p \leq 0.0001$ (****). Not significant; *ns*.

Figure 3. ABHD17 knockdown enhances localization and function of GFP-NOD2 at plasma membrane in HCT116 cells (A) *ABHD17A*, *ABHD17B* and *ABHD17C* have similar levels of expression (quantitation cycle (Cq) value assessed by qPCR) in HCT116 cells. *GAPDH* was used as a reference gene. The line across the boxplot depicts the mean. The whiskers represent the maximum and minimum values. **(B)** RT-qPCR of *ABHD17A*, *ABHD17B* and *ABHD17C* transcript levels in HCT116 cells treated with non-targeting small interfering RNA (siRNA) (grey), or ABHD17A siRNA alone (cyan), or ABHD17B siRNA alone (magenta), or ABHD17C siRNA alone (yellow), or ABHD17A/ABHD17B/ABHD17C siRNAs (orange) for 48h. **(C)** Confocal images showing the effects of siRNA-mediated knockdown of ABHD17 isoforms on localization of GFP-NOD2 (cyan) in HCT116. Scale bars, 5μm. **(D)** Quantification of GFP-NOD2 plasma membrane localization from images as in (C). **(e)** Immunoblots of phosphorylated- IkBα, NF-κB p65, and MAPK p38 in HCT116 cells. **(F-H)** Quantification of immunoblots as in (E). **(I & J)** Cytokine (GM-CSF and IL-8) levels in cell culture supernatants. All data are representative of at least three independent experiments. All error bars, mean values ±

SD. p-values for data in (D), (F), (G) & (H) were determined by one-way ANOVA followed by Dunnett's post hoc test or Tukey's multiple comparisons test. Statistical significance of data in (I & J) was determined by two-way ANOVA then Fisher's least significant difference (LSD) method for multiple comparisons. Group differences were considered significant for p≤0.05 (*), p≤0.01 (**), p≤0.001 (***) and p≤0.0001 (****). Not significant; *ns*.

Figure 4. Inhibition of ABHD17 enzymes rescues some deficiently palmitoylated NOD2 mutants (A) Confocal images showing localization of GFP-tagged L1007fs variant of NOD2 (cyan) transiently expressed in HCT116 cells treated with 100 μM PalmB and 2.5μM ABD957. **(B)** Confocal images showing localization of GFP-tagged L248R, R702W and A755V NOD2 variants in stably expressed in HCT116 cells treated with 40 μM THL, 100 μM PalmB, 2.5 μM ABD957 and ABHD17A/ABHD17B/ABHD17C siRNAs (triple KD). Scale bars, 5 μm. (**C-E**) Quantification of plasma membrane localization of NOD2 variants from images as in (B). **(F)** *S*-acylation levels of GFP-tagged NOD2 variants in HCT116 cells treated with THL, ABD957 or PalmB. *S*-acylated L248R, R702W and A755V GFP fusion proteins were detected in total cell lysates using acyl-RAC assay and immunoblot analysis. Immunoblots of phosphorylated- IKBα and MAPK p38 in HEK293T cells stably expressing **(G)** L248R **(H)** R702W **(I)** A755V. **(J & K)** Cytokine (IL-8 and TNFα) levels in cell culture supernatants. All data and immunoblots are representative of at least three independent experiments. All error bars, mean values ± SD. p-values for data were determined by one-way ANOVA followed by Dunnett's post hoc test or Tukey's multiple comparisons test. Group

differences were considered significant for $p \leq 0.05$ (*), $p \leq 0.01$ (**) and $p \leq 0.0001$ (****). Not significant; *ns*.

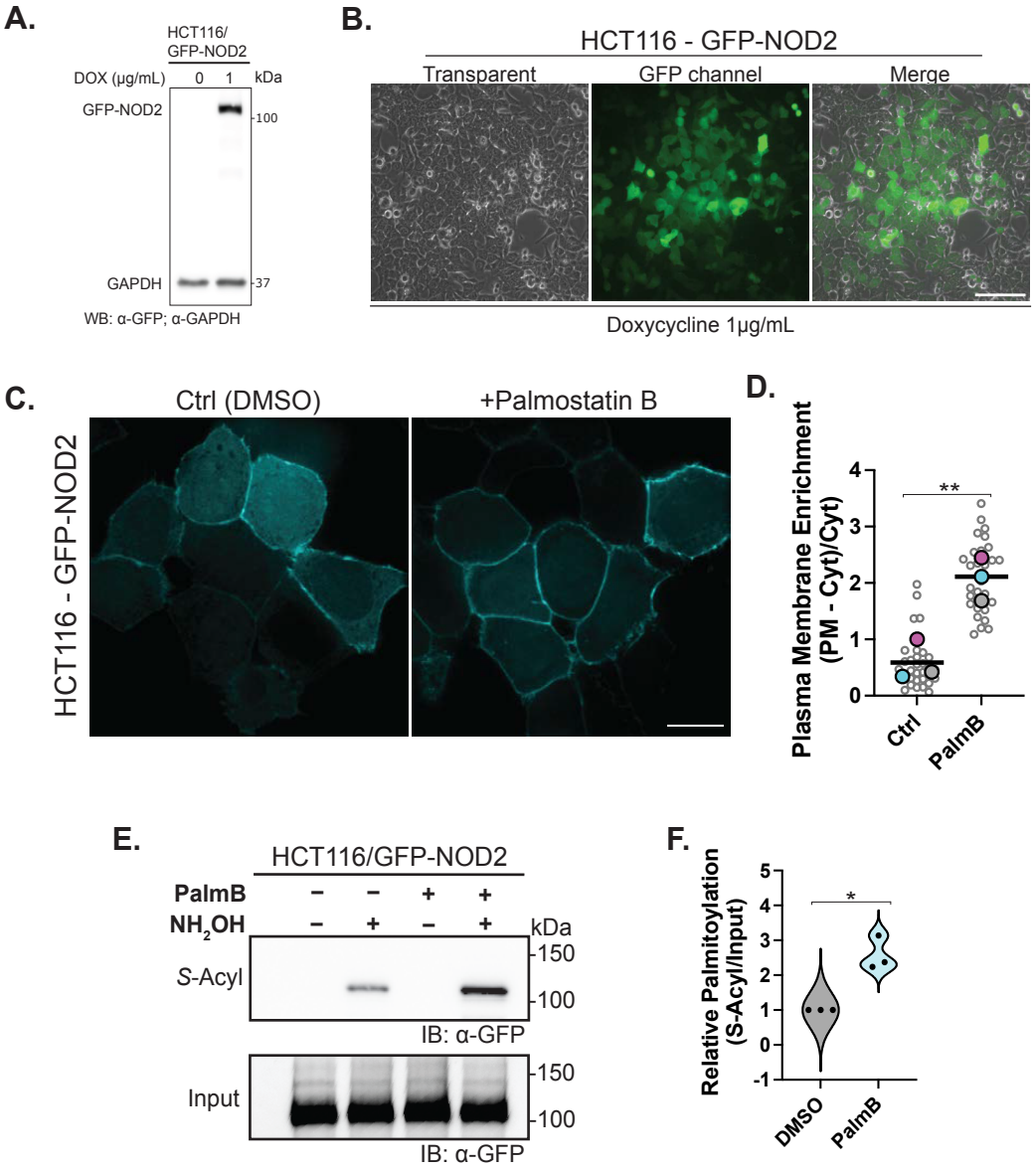
A.
HCT116/
GFP-NOD2
DOX (μg/mL)
0
1
kDa
GFP-NOD2
100
GAPDH
37
WB: α-GFP; α-GAPDH
B.
HCT116 - GFP-NOD2
Transparent
GFP channel
Merge
Doxycycline 1μg/mL
C.
Ctrl (DMSO)
+Palmostatin B
HCT116 - GFP-NOD2
D.
Plasma Membrane Enrichment
(PM - Cyt)/Cyt)
**
Ctrl
PalmB
E.
HCT116/GFP-NOD2
PalmB
NH2OH
kDa
S-Acyl
150
100
IB: α-GFP
Input
150
100
IB: α-GFP
F.
Relative Palmitoylation
(S-Acyl/Input)
*
DMSO
PalmB

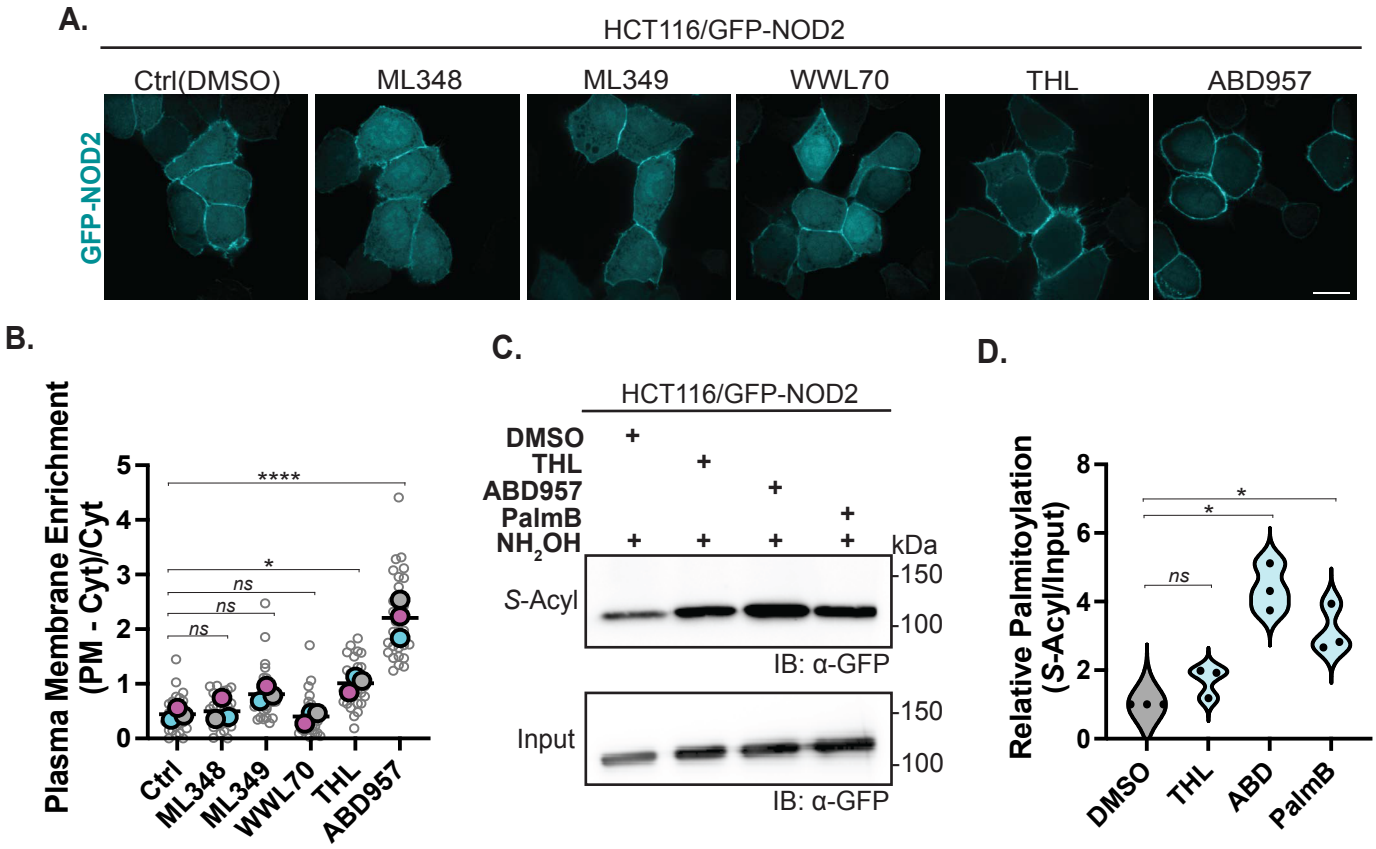
A.
HCT116/GFP-NOD2
Ctrl(DMSO)
ML348
ML349
WWL70
THL
ABD957
GFP-NOD2
B.
Plasma Membrane Enrichment (PM - Cyt)/Cyt
****
*
ns
ns
ns
Ctrl
ML348
ML349
WWL70
THL
ABD957
C.
HCT116/GFP-NOD2
DMSO
THL
ABD957
PalmB
NH2OH
kDa
S-Acyl
150
100
IB: α-GFP
Input
150
100
IB: α-GFP
D.
Relative Palmitoylation (S-Acyl/Input)
*
*
ns
DMSO
THL
ABD
PalmB

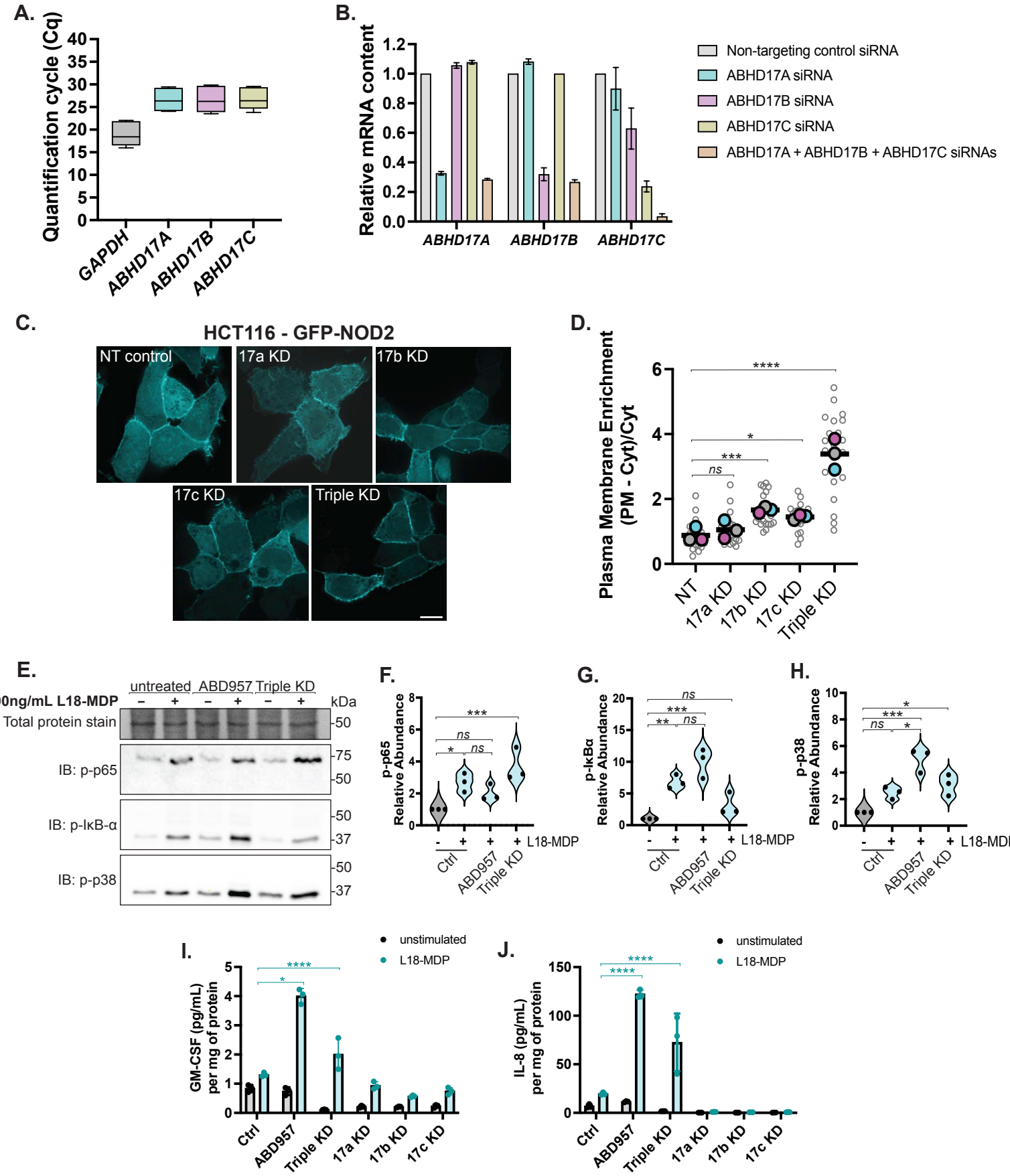
A.
Quantification cycle (Cq)
GAPDH
ABHD17A
ABHD17B
ABHD17C
B.
Relative mRNA content
ABHD17A
ABHD17B
ABHD17C
Non-targeting control siRNA
ABHD17A siRNA
ABHD17B siRNA
ABHD17C siRNA
ABHD17A + ABHD17B + ABHD17C siRNAs
C.
HCT116 - GFP-NOD2
NT control
17a KD
17b KD
17c KD
Triple KD
D.
Plasma Membrane Enrichment (PM - Cyt)/Cyt
NT
17a KD
17b KD
17c KD
Triple KD
E.
untreated
ABD957
Triple KD
100ng/mL L18-MDP
kDa
Total protein stain
IB: p-p65
IB: p-IκB-α
IB: p-p38
F.
p-p65 Relative Abundance
L18-MDP
Ctrl
ABD957
Triple KD
G.
p-IκBα Relative Abundance
H.
p-p38 Relative Abundance
I.
GM-CSF (pg/mL) per mg of protein
unstimulated
L18-MDP
Ctrl
ABD957
Triple KD
17a KD
17b KD
17c KD
J.
IL-8 (pg/mL) per mg of protein

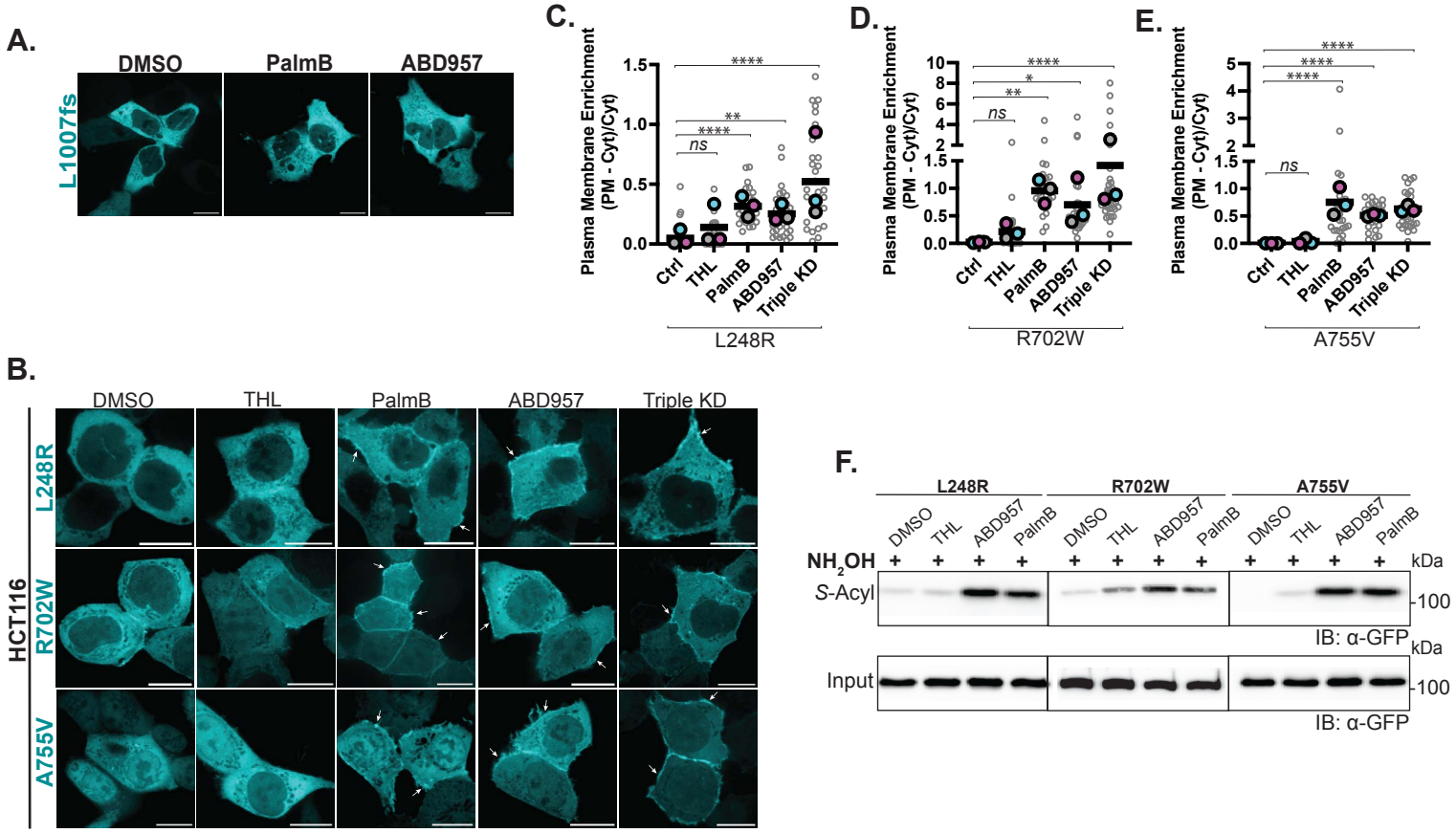
A.
DMSO
PalmB
ABD957
L1007fs
B.
DMSO
THL
PalmB
ABD957
Triple KD
HCT116
L248R
R702W
A755V
C.
Plasma Membrane Enrichment (PM - Cyt)/Cyt)
Ctrl
THL
PalmB
ABD957
Triple KD
L248R
D.
R702W
E.
A755V
F.
L248R
R702W
A755V
DMSO
THL
ABD957
PalmB
NH2OH
S-Acyl
Input
kDa
100
IB: α-GFP

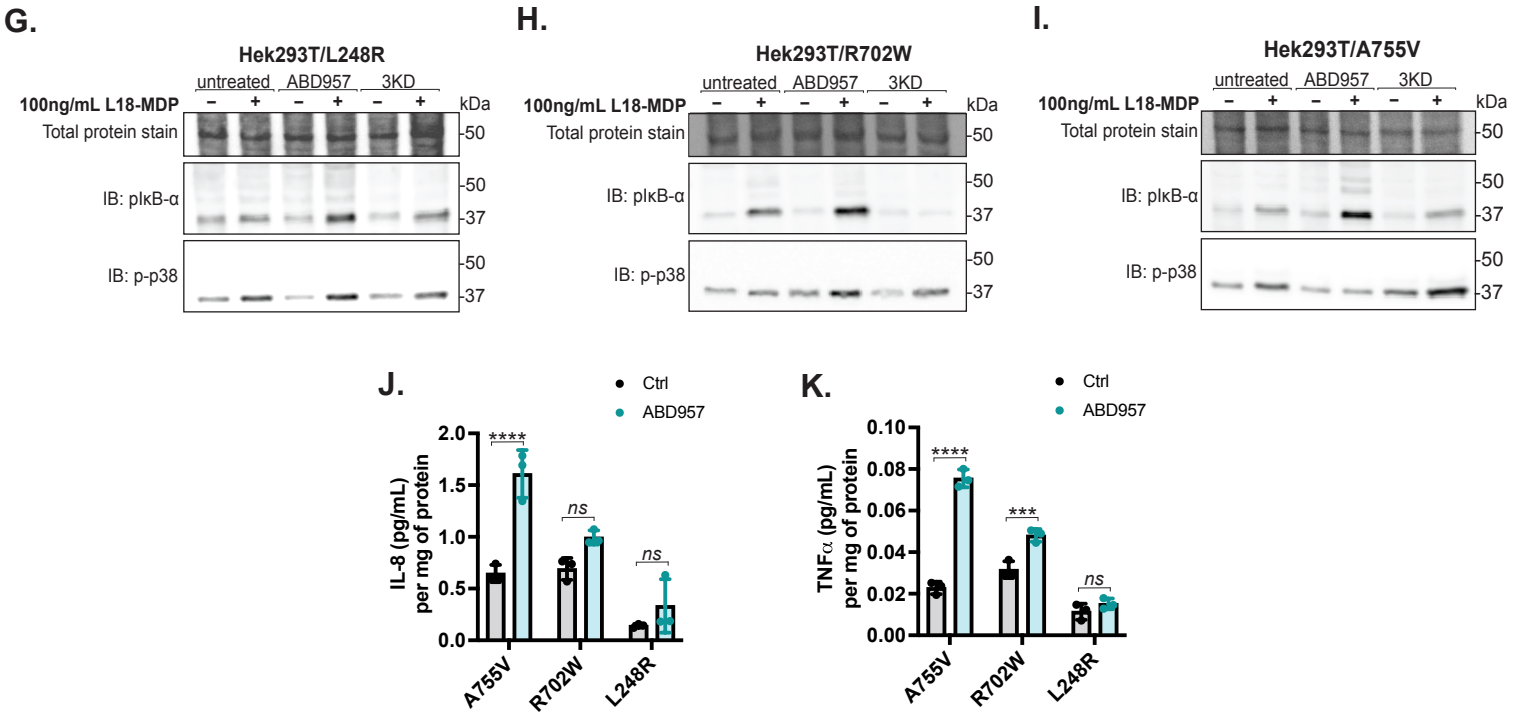
G.
Hek293T/L248R
H.
Hek293T/R702W
I.
Hek293T/A755V
untreated
ABD957
3KD
100ng/mL L18-MDP
Total protein stain
IB: pIκB-α
IB: p-p38
kDa
50
37
J.
Ctrl
ABD957
IL-8 (pg/mL) per mg of protein
A755V
R702W
L248R
K.
TNFα (pg/mL) per mg of protein